IV. 研究成果の刊行物・別冊

ARTICLE

SMOC1 Is Essential for Ocular and Limb Development in Humans and Mice

Ippei Okada,[1,14] Haruka Hamanoue,[1,2,14] Koji Terada,[3] Takaya Tohma,[4] Andre Megarbane,[5] Eliane Chouery,[5] Joelle Abou-Ghoch,[5] Nadine Jalkh,[5] Ozgur Cogulu,[6] Ferda Ozkinay,[6] Kyoji Horie,[7] Junji Takeda,[7,8] Tatsuya Furuichi,[9,10] Shiro Ikegawa,[9] Kiyomi Nishiyama,[1] Satoko Miyatake,[1] Akira Nishimura,[1] Takeshi Mizuguchi,[1,15] Norio Niikawa,[11,12] Fumiki Hirahara,[2] Tadashi Kaname,[13] Koh-ichiro Yoshiura,[12] Yoshinori Tsurusaki,[1] Hiroshi Doi,[1] Noriko Miyake,[1] Takahisa Furukawa,[3] Naomichi Matsumoto,[1,*] and Hirotomo Saitsu[1,*]

Microphthalmia with limb anomalies (MLA) is a rare autosomal-recessive disorder, presenting with anophthalmia or microphthalmia and hand and/or foot malformation. We mapped the MLA locus to 14q24 and successfully identified three homozygous (one nonsense and two splice site) mutations in the SPARC (secreted protein acidic and rich in cysteine)-related modular calcium binding 1 (SMOC1) in three families. Smoc1 is expressed in the developing optic stalk, ventral optic cup, and limbs of mouse embryos. Smoc1 null mice recapitulated MLA phenotypes, including aplasia or hypoplasia of optic nerves, hypoplastic fibula and bowed tibia, and syndactyly in limbs. A thinned and irregular ganglion cell layer and atrophy of the anteroventral part of the retina were also observed. Soft tissue syndactyly, resulting from inhibited apoptosis, was related to disturbed expression of genes involved in BMP signaling in the interdigital mesenchyme. Our findings indicate that SMOC1/Smoc1 is essential for ocular and limb development in both humans and mice.

Introduction

Microphthalmia with limb anomalies (MLA [MIM 206920]), also known as Waardenburg anophthalmia syndrome or ophthalmoacromelic syndrome, is a rare autosomal-recessive disorder first described by Waardenburg.[1] It is characterized by ocular anomalies ranging from mild microphthalmia to true anophthalmia and by limb anomalies such as oligodactyly, syndactyly, and synostosis of the 4th and 5th metacarpals.[2–4] The genetic cause for MLA has remained unknown.

It is widely known that secreted signaling molecules such as Sonic hedgehog (Shh), wingless-type MMTV integration site family (Wnt), transforming growth factor β (Tgf-β), bone morphogenetic proteins (Bmps), and fibroblast growth factor (Fgf) are involved in the development of many organs and tissues, including the eyes and limbs.[5,6] In particular, mutations in BMP4 (MIM 112262) have resulted in anophthalmia with systemic manifestations, including polydactyly and/or syndactyly (also known as micropthalmia, syndromic 6, MCOPS6 [MIM

607932]),[7] highlighting importance of BMP signaling in both the developing eye and limb.

SMOC1 (MIM 608488), which encodes SPARC (secreted protein acidic and rich in cysteine)-related modular calcium binding 1, is a member of the SPARC (also known as BM-40) matricellular protein family that modulates cell-matrix interaction by binding to many cell-surface receptors, the extracellular matrix, growth factors, and cytokines.[8,9] SMOCs are extracellular glycoproteins with five domains: an N-terminal follistatin-like (FS) domain, two thyroglobulin-like (TY) domains, a domain unique to SMOC, and an extracellular calcium-binding (EC) domain.[9] SMOC1 is widely expressed in various tissues with localization to basement membranes.[9,10] Although the biological function of SMOC1 remains largely unknown, it has been recently reported that Xenopus smoc protein, the ortholog of human SMOC1, acts as a BMP antagonist,[11] suggesting that human SMOC1 can also modulate BMP signaling.

Here, we demonstrate that SMOC1 mutations cause MLA. We also show that Smoc1 null mice recapitulated

[1]Department of Human Genetics, Yokohama City University Graduate School of Medicine, 3-9 Fukuura, Kanazawa-ku, Yokohama 236-0004, Japan; [2]Department of Obstetrics and Gynecology, Yokohama City University Graduate School of Medicine, 3-9 Fukuura, Kanazawa-ku, Yokohama 236-0004, Japan; [3]Department of Developmental Biology, Osaka Bioscience Institute, 6-2-4 Furuedai, Suita, Osaka 565-0874, Japan; [4]Division of Pediatrics, Okinawa Prefectural Nanbu Medical Center & Children's Medical Center, 118-1 Ikyoku, Arakawa, Haebaru, Okinawa 901-1193, Japan; [5]Medical Genetics Unit, St. Joseph University, Beirut 1104-2020, Lebanon; [6]Department of Pediatrics, Ege University Faculty of Medicine, 35100 Bornova-Izmir, Turkey; [7]Department of Social and Environmental Medicine, Graduate School of Medicine, Osaka University, 2-2 Yamadaoka, Suita, Osaka 565-0871, Japan; [8]Center for Advanced Science and Innovation, Osaka University, 2-1 Yamadaoka, Suita, Osaka 565-0871, Japan; [9]Laboratory for Bone and Joint Disease, Center for Genomic Medicine, RIKEN, 4-6-1 Shirokanedai, Minato-ku, Tokyo 108-8639, Japan; [10]Laboratory Animal Facility, Research Center for Medical Sciences, Jikei University School of Medicine, 3-25-8, Nishi-Shimbashi, Minato-ku, Tokyo 105-8461, Japan; [11]Research Institute of Personalized Health Sciences, Health Sciences University of Hokkaido, Ishikari-Tobetsu, Hokkaido 061-0293, Japan; [12]Department of Human Genetics, Nagasaki University Graduate School of Biomedical Sciences, Sakamoto 1-12-4, Nagasaki 852-8523, Japan; [13]Department of Medical Genetics, University of the Ryukyus Faculty of Medicine, 207 Uehara, Nishihara, Okinawa 903-0215, Japan
[14]These authors contributed equally to this work
[15]Current address: Laboratory of Biochemistry and Molecular Biology, National Cancer Institute, National Institutes of Health, Building 37, Room 6050, Bethesda, MD 20892, USA
*Correspondence: naomat@yokohama-cu.ac.jp (N.M.), hsaitsu@yokohama-cu.ac.jp (H.S.)

MLA phenotypes, indicating that *SMOC1* plays essential roles in both eye and limb development in humans and mice.

Subjects and Methods

Subjects

A total of four families with one or two cases of MLA were analyzed in this study, including three previously reported families (A, B, and C).[12,13] Family X from Turkey, which has been previously described,[14] was newly recruited to this study. Detailed clinical information of all the patients is available in the literature,[12,14] and phenotypes of patients with confirmed mutations are summarized in Table S1 (available online). A total of five affected and 16 unaffected members from the four families were analyzed in the linkage study. Genomic DNA was obtained from peripheral-blood leukocytes with the use of QuickGene 610-L (Fujifilm, Tokyo, Japan) after informed consent had been given. Experimental protocols were approved by the institutional review board of Yokohama City University School of Medicine.

SNP Genotyping, and Fine Mapping with Short Tandem Repeat Markers

Whole-genome SNP genotyping, with the use of GeneChip Human Mapping 50K Array XbaI (Affymetrix, Santa Clara, CA), and fine mapping of possible candidate regions, with the use of additional microsatellite markers, were performed as previously described.[12,15] The list of primers used for fine mapping is presented in Table S2.

Linkage Analysis

Multipoint linkage analyses using aligned SNPs were performed with ALLEGRO software.[16] Two-point linkage analyses of candidate regions were performed with the LINKAGE package MLINK (FASTLINK software, version 5.1). In each program, an autosomal-recessive model of inheritance with complete penetrance and a disease-allele frequency of 0.001 were applied.

Mutation Analysis of Candidate Genes

All coding exons and exon-intron boundaries of *RAD51L1* (MIM 602948), *ACTN1* (MIM 102575), *ERH* (MIM 601191), *SRSF5* (MIM 600914), *DCAF5* (MIM 603812), *COX16*, *EXD2*, *GALNTL1*, *SLC39A9*, *KIAA0247*, *MED6* (MIM 602984), *TTC9* (MIM 610488), *MAP3K9* (MIM 600136), and *SMOC1* (transcript variant 1, GenBank accession number NM_001034852.1) were analyzed in the probands of families A, C, and X. The transcript variant 2 of *SMOC1* (GenBank accession number NM_022137.4) is 3 bp shorter than the variant 1, leading to an in-frame amino acid deletion at position 431. PCR was cycled 35 times at 94°C for 30 s, at 60°C for 30 s, and at 72°C for 30–90 s in a total volume of 20 μl containing 30 ng genomic DNA as a template, 0.5 μM forward and reverse primers, 200 μM each deoxyribonucleotide triphosphate (dNTP), 1 × ExTaq buffer, and 0.25 U ExTaq (Takara). All primers were designed with Primer3 software. Detailed information of primers is available upon request. PCR products were purified with ExoSAP (USB) and sequenced with BigDye Terminator 3.1 (Applied Biosystems) on a 3100 Genetic Analyzer. Sequences of patients were compared to reference genome sequences in the UCSC Genome Browser (February 2009

assembly) with Seqscape software, version 2.1 (Applied Biosystems).

Animals

Smoc1 mutant mice, created with the use of the *Sleeping Beauty* transposon system, have been previously described.[17] Line PV384 was provided by the RIKEN BioResource Center through the National BioResource Project of MEXT, Japan. Three independent mouse lines (no. 1 to no. 3), each with a single insertion in intron 1 of *Smoc1*, were bred as heterozygotes. Lines 1 and 3 were backcrossed for at least four generations to a C57BL/6J background. Line 2 was maintained with a mixed background of C57BL/6J and ICR. We mainly analyzed line 1, but we confirmed similar phenotypes in lines 2 and 3. Animals were housed in accordance with protocols approved by the Institutional Animal Care and Use Committee at Yokohama City University, School of Medicine. PCR genotyping of mice was performed with the use of genomic DNA from yolk-sac, ear, or tail biopsies. The following primers were used: PV384-WF, 5′-AAAGGCTGGGAATTGTTTG A-3′; PV384-WR, 5′-TGCAGCTGAAACTGTCTCTCC-3′; PV384-MF, 5′-TGTCCTAACTGACTTGCCAAA-3′. The PV384-WF/PV384-WR primers amplified a 441 bp wild-type (WT) product, and the PV384-MF/PV384-WR primers amplified a 218 bp mutant product.

Southern Hybridization

Genomic DNA was extracted from livers or tail biopsies of PV384 heterozygous (*Smoc1*$^{Tp/+}$) mice via standard protocols. The gene-trap insertions were analyzed by Southern hybridization with the use of 10 μg of SacI-, NdeI-, BglII-, and EcoRI-digested DNA. The probe (451 bp), which hybridized to the internal ribosome entry site (IRES) in the gene-trap vector, was synthesized with the DIG PCR Probe Synthesis Kit (Roche) with the use of the following primers: 5′-CTAACGTTACTGGCCGAAGC-3′ and 5′-CCCAGATCAGATCCCATACAA-3′. Hybridization, washing, and detection of probes were performed according to the manufacturer's protocol. Images were captured with the FluorChem system (Alpha Innotech).

Cloning of Gene-Trap Insertion Sites

After identification of aberrant DNA fragments by Southern hybridization, NdeI-, SacI-, and EcoRI-digested DNA from PV384 mice was fractionated by electrophoresis, and appropriately sized fragments containing *Ol1* (other locus 1), *Ol2*, and *Ol3* were isolated with a QIAEXII Gel Extraction Kit (QIAGEN). The isolated DNA was self-ligated by Ligation High ver.2 (Toyobo), precipitated with ethanol, and dissolved in 20 μl EB buffer (QIAGEN). Inverse PCR was performed in 25 μl reactions, containing 2 μl ligated DNA, 1 × PCR buffer for KOD FX, 0.4 mM each dNTP, 0.5 μM each primer, and 0.5 U KOD FX DNA polymerase (Toyobo). Primers common to *Ol1*, *Ol2*, and *Ol3* were as follows: Inv-F, 5′- AT CGCCAGTTCTGTATGAACGGTCTGGTCTT-3′; Inv-R, 5′-CCCTC TTTACGTGCCAGCCATCTTAGAGATAC-3′. Confirmatory PCR of gene-trap insertion sites for *Ol1*, *Ol2*, and *Ol3* loci was performed with the use of the following primers: *Ol1*-F, 5′-GAGTGGTATTCA TTGGATTCTGCTGAT-3′; *Ol2*-F, 5′-AAATCCAGCTGGCCAACAGA CTAAG-3′; *Ol3*-F, 5′-TTGCCGGGTAGACTCTATCAAGAACCA-3′; TBAL-R, 5′-CTTGTGTCATGCACAAAGTAGATGTCC-3′. Primer sets of *Ol1*-F/TBAL-R, *Ol2*-F/TBAL-R, and *Ol3*-F/TBAL-R could amplify 175 bp, 607 bp, and 767 bp products, respectively. These PCR primer pairs were also used for genotyping of mice harboring a single insertion at the *Smoc1* locus.

Confirmation of Promoter- and Poly(A)-Trapped Transcripts

Whole embryos at embryonic day 10.5 (E10.5) and E11.5 were stored in RNAlater solution (QIAGEN). Total RNA was extracted from WT, $Smoc1^{Tp/+}$, and $Smoc1^{Tp/Tp}$ embryos with the use of RNeasy Plus Mini (QIAGEN). One microgram total RNA was subjected to reverse transcription with the use of a PrimeScript 1st Strand Synthesis Kit with random hexamers (Takara). A control reaction with no reverse transcriptase was included in each experiment. PCR was performed in 20 μl reactions, containing 1 μl cDNA, 1 × PCR Buffer for KOD FX, 0.4 mM each dNTP, 0.3 μM each primer, and 0.4 U KOD FX (Toyobo). Primers used are listed below: Smoc1-F, 5′-GTCCCCACCTCCCCAAGTGCTTTGA-3′; LacZ-R, 5′-TGCCAAAAGACGGCAATATGGTGGAAA-3′; GFP-F, 5′-T CACATGGTCCTGCTGGAGTTCGTGAC-3′; Smoc1-R, 5′-ACACT TGCTCTGGCCAGCATCTTTGCAT-3′. Primer sets of Smoc1-F/ Smoc1-R, Smoc1-F/LacZ-R, and GFP-F/Smoc1-R could amplify native Smoc1 (366 bp), promoter-trapped transcripts (Tp-LacZ, 500 bp) and poly(A)-trapped transcripts (Tp-GFP, 308 bp), respectively. The PCR conditions were 98°C for 10 s, 68°C for 1 min, for 30 cycles. Primers for ACTB[18] were used as an internal control. PCR for ACTB was cycled 20 times at 94°C for 20 s, 60°C for 20 s, and 72°C for 30 s in a total volume of 10 μl containing 0.5 μl cDNA, 0.4 μM each primer, 0.2 mM each dNTP, 1 × ExTaq buffer, and 0.5 U ExTaq HS (Takara). All PCR products were electrophoresed on 2% agarose gels.

In Situ Hybridization

Embryos were collected between E9.5 and E13.5. Whole-mount in situ hybridization was carried out as previously described.[19,20] Two fragments of Smoc1 cDNA were obtained as probes by RT-PCR, with the use of total RNA extracted from livers of E16.5 mouse embryos, and subcloned into pCR4-TOPO (Invitrogen). Primer sequences were as follows: probe 1-F, 5′-GTCTGCTCACGCCCC ACT-3′; probe 1-R, 5′-CCTGAACCATGTCTGTGGTG-3′; probe P-F, 5′-CAGGAACAGGAAAGGGAAGA-3′; probe P-R, 5′-AAGGGAAA ACCACACAGCAC-3′. PCR products were 1023 bp and 1578 bp, corresponding to nucleotide positions 275–1297 and 1849–3426 of the mouse Smoc1 cDNA (GenBank accession number NM_001146217.1), respectively. The cDNA fragment amplified with probe P-F and probe P-R primers was identical to the probe used in a previous report.[21] Digoxigenin-labeled sense and antisense riboprobes were synthesized with the use of a digoxigenin RNA labeling kit (Roche). These two different antisense probes demonstrated identical staining patterns, and the control sense probes showed no staining. The expression pattern was confirmed with more than three embryos. In addition, the following probes were used: Bmp2 (gift from Y. Takahashi),[22] Sox9 (gift from A. Yamada),[22] Bmp7 (gift from E.J. Robertson), and Msx2 (gift from Dr. R.E. Maxson, Jr). The numbers of embryos examined were as follows (numerical quantity for WT, $Smoc1^{Tp/+}$, and $Smoc1^{Tp/Tp}$, respectively, shown in parentheses): Msx2 (2, 1, 3) at E11.5; Bmp2 (3, 0, 3), Bmp7 (3, 0, 3), Msx2 (3, 0, 3), and Sox9 (2, 1, 3) at E12.5; Bmp2 (1, 2, 3), Bmp7 (2, 1, 3), Msx2 (1, 2, 3), and Sox9 (1, 3, 4) at E13.5. Stained embryos were cleared in glycerol to enable images to be produced with a VHX-1000 digital microscope (Keyence).

Histology

Heads of embryos and newborns were fixed overnight in 4% paraformaldehyde in PBS at 4°C. These embryos were then washed in PBS. Frozen samples were serially sectioned at 16 μm (E14.5) and 20 μm (P0). The numbers of eyes examined (WT, $Smoc1^{Tp/+}$,

$Smoc1^{Tp/Tp}$) were as follows: coronally sectioned at E14.5 (8, 10, 12), coronally sectioned at P0 (8, 10, 6), horizontally sectioned at P0 (2, 2, 4). For evaluation of ventral atrophy of the retina, only the coronally sectioned eyes were used. TB staining was performed according to standard protocols. Forelimbs of mice were fixed in 4% paraformaldehyde in PBS, decalcified in 10% EDTA, and embedded in paraffin. Forelimbs were serially sectioned at 4 μm and stained with hematoxylin and eosin.

Evaluation of Optic Nerve Diameter

The palatine and orbital bones were carefully removed to expose the optic chiasm and optic nerve. During the dissection process, 4% paraformaldehyde in PBS was frequently applied onto the gaps between the bone and optic nerve. Xylene cyanol was applied to enhance the outline of optic nerves at poastnatal day 0 (P0). Photographs of optic nerves were taken with a VHX-1000 digital microscope, and the diameter was measured for right and left optic nerves with the bundled software included with the VHX-1000 instrument.

Skeletal Staining

For skeletal preparations, mice were fixed in 99.5% ethanol after removal of the skin and viscera. Cartilage tissues were stained with 0.015% alcian blue and 20% acetic acid in 75% ethanol for three days at 37°C. After dehydration with 99.5% ethanol for three days, bones were stained with 0.002% alizarin red in 1% KOH. Then skeletons were cleared in 1% KOH for several weeks. For P14 mice, soft tissues were dissolved in 2% KOH before alizarin red staining.

Nile Blue Staining

For the study of apoptosis of hindlimbs at E13.5 and E14.5, Nile blue (NB) staining was performed on the basis of a previously described protocol,[23] except that staining was performed at 37°C (not room temperature). Apoptosis was determined by NB-stained (deceased) cells. After rinsing in Tyrode solution, hindlimbs of control (WT and heterozygous littermates) and homozygous mice were evaluated. Photographs of dorsal aspects were taken with a VHX-1000 digital microscope. Experiments were repeated three times, and reproducible representative results are presented.

Statistical Analysis

Statistical analyses were performed with the use of non-repeated-measures ANOVA followed by Dunnett's post hoc test. The results are given as mean ± standard deviation, and the threshold p value for statistical significance was 0.01.

Results

Identification of Homozygous SMOC1 Mutations

We have previously mapped the MLA locus to a 422 kb region at 10p11.23 by analyzing three families (one Japanese family [A] and two Lebanese families [B and C]). This region contained only one gene, MPP7, in which no mutations were found.[12] After a new Turkish family (X) was added to the analysis, the MLA locus was again searched by homozygosity mapping to the consanguineous families (X, B, and C) and haplotype mapping to family A for detection of compound-heterozygous mutations; however, we could not detect any common regions

among the four families. We then focused on identifying common regions in any three of the four families to allow for locus heterogeneity (Table S3).

A locus at 14q24.1-q24.2, which showed the highest LOD score (3.936) among the candidate regions larger than 2.0 Mb, was highlighted among families A, C, and X. This locus was analyzed with the use of additional microsatellite markers, and a 3.0 Mb region containing 24 genes was identified (Figures 1A and 1B). A total of 14 genes were sequenced, and homozygous mutations were found in SMOC1: c.718C>T (p.Gln240X) in family A, c.664+1G>A in family C, and c.378+1G>A in family X (Figures 1C and 1D). All of these homozygous mutations were cosegregated with the disease phenotype, and the parents of the individuals with these mutations were heterozygous carriers (Figure 1C). We could not find any mutations in SMOC1 in family B, in which MLA is unlinked to the 14q24.1-q24.2 locus. Interestingly, in family A haplotypes of paternal and maternal alleles, each having the same mutation, are completely different (data not shown), suggesting that the same mutation may have occurred in separate events. The c.718C>T mutation was not detected in 289 healthy Japanese controls, including 100 Okinawa islanders. The other two mutations were not detected in ethnically matched controls (54 Lebanese and 99 Turkish subjects, respectively), nor in 289 Japanese controls. The two splice-donor-site mutations (c.664+1G>A and c.378+1G>A) are predicted to abolish a donor site, as predicted by ESE-finder, NetGene2, HSF2.4.1, SpliceView, and BDGP analysis (Table S4). Thus, the three mutations are likely to lead to a loss of functional SMOC1.

Smoc1 Expression in the Developing Eye and Limb in Mice

For the examination of Smoc1 expression in the developing eye and limb, whole-mount in situ hybridization of mouse embryos was performed. Smoc1 was expressed in the forebrain, midbrain, hindbrain, pharyngeal arch, somites, and forelimb buds at E9.5 (Figure 2A). At E10.5, Smoc1 expression was observed in the optic stalk (Figure 2B), and at E11.5, expression was localized to the closure site of the optic cup (Figure 2C). Expression of Smoc1 in developing limbs between E10.5 and E11.5 was observed in both dorsal and ventral regions, with a broader pattern of expression in dorsal regions, but expression was not detected in the most anterior, posterior, and distal parts of limb buds (Figures 2D and 2E). Expression coinciding with chondrogenic condensation was observed at E12.5 (Figure 2F), and expression then became restricted to future synovial joint regions at E13.5 (Figure 2G). This dynamic expression suggests that Smoc1 plays a critical role in ocular and limb development.

Ocular and Limb Anomalies in Smoc1 Null Mice

To investigate the pathological basis of MLA due to the loss of SMOC1 function, we obtained Smoc1 mutant mice, PV384.[17] PV384 mice possess gene-trap insertions in the Smoc1 locus and in three other loci. After PV384 mice were bred with C57BL/6J or ICR mice, we obtained three independent lines (no. 1 to no. 3), each with a sole insertion in intron 1 of Smoc1 (Figure S1). We mainly analyzed line 1, but we confirmed similar phenotypes in lines 2 and 3. Heterozygous mutant mice (Smoc1$^{Tp/+}$) were healthy and fertile. Homozygous mice (Smoc1$^{TP/TP}$) were null mutants, as they showed no native transcript of Smoc1 (Figure S1E). Homozygous mice were viable at P0; however, they did not survive beyond the first 3 wks of life (Figure 3B). Their growth was retarded in comparison to WT and heterozygous littermates at P0 and P14 (Figures 3A and 3C). Developmental defects in eyes and optic nerves were evident at E14.5. Homozygous mice had relatively small eyes, and histological examinations revealed aplasia or hypoplasia of optic nerves (in 10 of 12 optic nerves), atrophy of the anteroventral part of the retina (in 11 of 12 eyes), and extension of the retinal pigmented epithelium (RPE) to the optic nerve (in 10 of 12 eyes) (Figures 3D–3I). These abnormalities were also observed at P0 (aplasia or hypoplasia of optic nerves [in 7 of 10 optic nerves], retinal atrophy [in 6 of 6 eyes], and RPE extension [in 3 of 6 eyes with identifiable optic nerves]) (Figures 3J–3M). WT or heterozygous littermates did not show any such abnormalities, except that a few eyes of heterozygous mice showed extension of the RPE at E14.5, but not at P0 (in 2 of 10 and 0 of 12 eyes, respectively). Toluidine blue (TB) staining showed ganglion cell layers that were thinned and irregular to varying degrees in homozygous mice, suggesting a reduced number of retinal ganglion cells (Figures 3J–3K′). Thus, Smoc1 is required for axon sprouting, elongation, or maintenance of retinal ganglion cells.[24] Hypoplasia of optic nerves was further quantitatively confirmed by macroscopic examination: the average diameter of optic nerves of homozygous mice was significantly smaller than that of WT and heterozygous littermates at P0 and P14 (Figures 3L–3Q). These data clearly demonstrate that loss of Smoc1 in mice affects development of the body, retina, and optic nerves, in a manner similar to that seen in MLA patients.[3,4]

Newborn homozygous mice could be readily identified by their hindlimb syndactyly and pes valgus, whereas no abnormalities were observed in WT and heterozygous pups (Figure 4 and Table 1). Interestingly, the severity of syndactyly varied between mouse lines: line 1 exclusively showed soft tissue syndactyly, whereas line 2 frequently showed four digits (Figures 4F and 4J). Skeletal preparations with alcian blue and alizarin red revealed that the foot with four digits had four phalanx and five metatarsals with fusion to each other (Figure 4K). Thus the Smoc1 null mutation resulted in a spectrum of phenotypes, from soft tissue syndactyly to four fused digits, probably due to different genetic backgrounds. Bowed tibiae and hypoplastic fibulae were also consistently observed in homozygous mice (Figures 4H and 4L). The articulation between
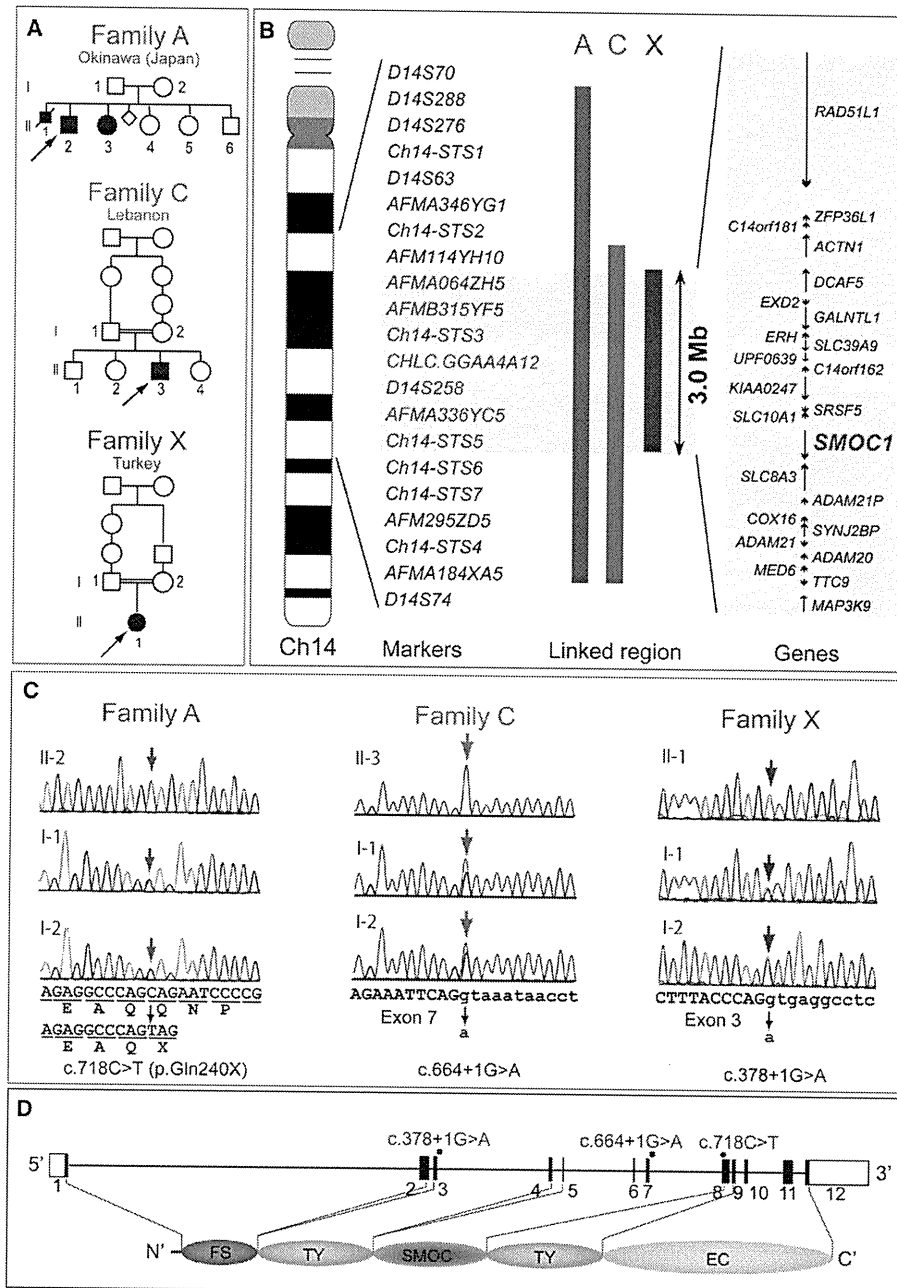
Figure 1. Genetic Analysis of Three Families with Members Affected by Microphthalmia with Limb Anomalies

(A) Pedigrees of the three families.

(B) Linkage analysis with SNPs and microsatellite markers on chromosome 14. From left to right: chromosome ideogram, genetic markers, linked regions of the three families, and genes mapped to the shortest overlapping linked region (between AFM114YH10 and Ch14-STS6 [UCSC coordinates, Feb. 2009: chromosome 14: 68,388,190–71,347,908 bp]).

(C) Sequences of mutations identified in each family. Affected patients in family A have a homozygous nonsense mutation (c.718C>T). Patients in families C and X have distinct homozygous splice-donor site mutations (c.664+1G>A and c.378+1G>A, respectively). For all mutations, parents of affected patients are heterozygous carriers, without exception. Sequences of the exon and intron are presented in upper and lower cases, respectively.

(D) At the top is a depiction of a schematic representation of SMOC1 consisting of 12 exons (UTR and coding exons are indicated by open and filled rectangles, respectively). The locations of three mutations are indicated by red dots. At the bottom, the functional domains of SMOC1 are depicted. Abbreviations are as follows: FS, the follistatin-like domain; TY, the thyroglobulin-like domain; SMOC, the domain unique to SMOC; and EC, the extracellular calcium-binding domain.
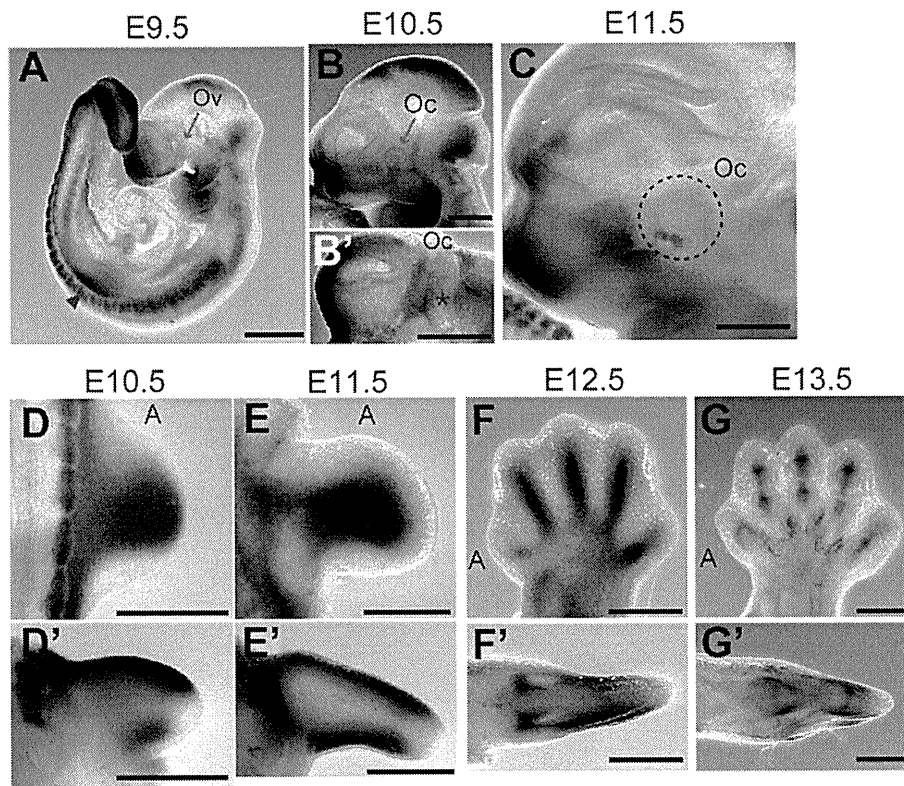
Figure 2. *Smoc1* **Expression in Mouse Embryos**
Lateral views of embryos (A–C) and a ventral view of the left part of the head (B', lateral view is shown at the top).
(A) At E9.5, *Smoc1* was expressed in the forebrain, midbrain, hindbrain, pharyngeal arch, somites, and forelimb buds (magenta arrowhead), but not in the optic vesicle (Ov, blue arrow).
(B and B') Expression in the optic stalk became evident at E10.5 (magenta asterisks), but was not evident in the optic cup (Oc, blue arrow).
(C) Expression was restricted to the closure site of the optic cup (dashed circle) at E11.5.
(D–G) Dorsal and (D'–G') posterior view of the right hindlimbs (dorsal view is shown at the top in D'–G'). The anterior side is indicated by an A. (D and D') At E10.5, *Smoc1* was more widely expressed in the dorsal part of the limb bud than in the ventral part. *Smoc1* expression is undetected in the most anterior, posterior, and distal parts of the limb bud. (E and E') At E11.5, ventral expression was broader than that in the previous stage. (F and F') At E12.5, expression was detected in areas consistent with chondrogenic condensation. (G and G') At E13.5, *Smoc1* expression became restricted to future joint regions. Scale bar represents 500 μm.

tibia/fibula and calcanea of homozygous mice appeared malpositioned (Figures 4G and 4K), which might contribute to pes valgus. At P14, soft tissue syndactyly was also evident in most forelimbs of homozygous mice (Figures 4M–4O). Moreover, hindlimbs of homozygous mice showed synostosis between the 4th and 5th metatarsals (Figure 4T), which is observed in both the hands and the feet of MLA patients. Thus, many limb anomalies of MLA patients were recapitulated in *Smoc1* null mice (Table S1).

Reduced Interdigital Apoptosis and Disturbed BMP Signaling
Among the various abnormalities caused by loss of *Smoc1* function, we focused on soft tissue syndactyly, which was commonly observed in both fore- and hindlimbs of null mutants. It is possible that the syndactyly is caused by failed apoptotic regression of the interdigital mesenchyme. To examine this hypothesis, hindlimbs were stained with NB sulfate at E13.5 and E14.5, the time

when interdigital apoptosis is most evident. In control embryos (WT and heterozygous littermates), NB-stained apoptotic cells were identified in the interdigital mesenchyme, where regression of the interdigital webbing occurs in the distal region (Figures 5A and 5C). By contrast, the number of apoptotic cells in the mesenchyme between digits 2 and 3 and digits 3 and 4 was dramatically reduced in homozygous mice at E13.5 and E14.5, along with persistent webbing in the distal region (Figures 5B and 5D, magenta asterisk). BMP signaling is involved in apoptosis of the interdigital mesenchyme.[25,26] *Bmp2*, *Bmp7*, and *Msx2*, a direct target of BMP signaling, were strongly expressed in the interdigital mesenchyme of control hindlimbs at both E12.5 and E13.5. However, the expression of these three genes was profoundly reduced and perturbed in hindlimbs of homozygous mice (Figures 5E–5J). These data suggest that inhibition of apoptosis is spatiotemporally correlated to reduced and/or disturbed expression of genes involved in BMP signaling in the interdigital mesenchyme.
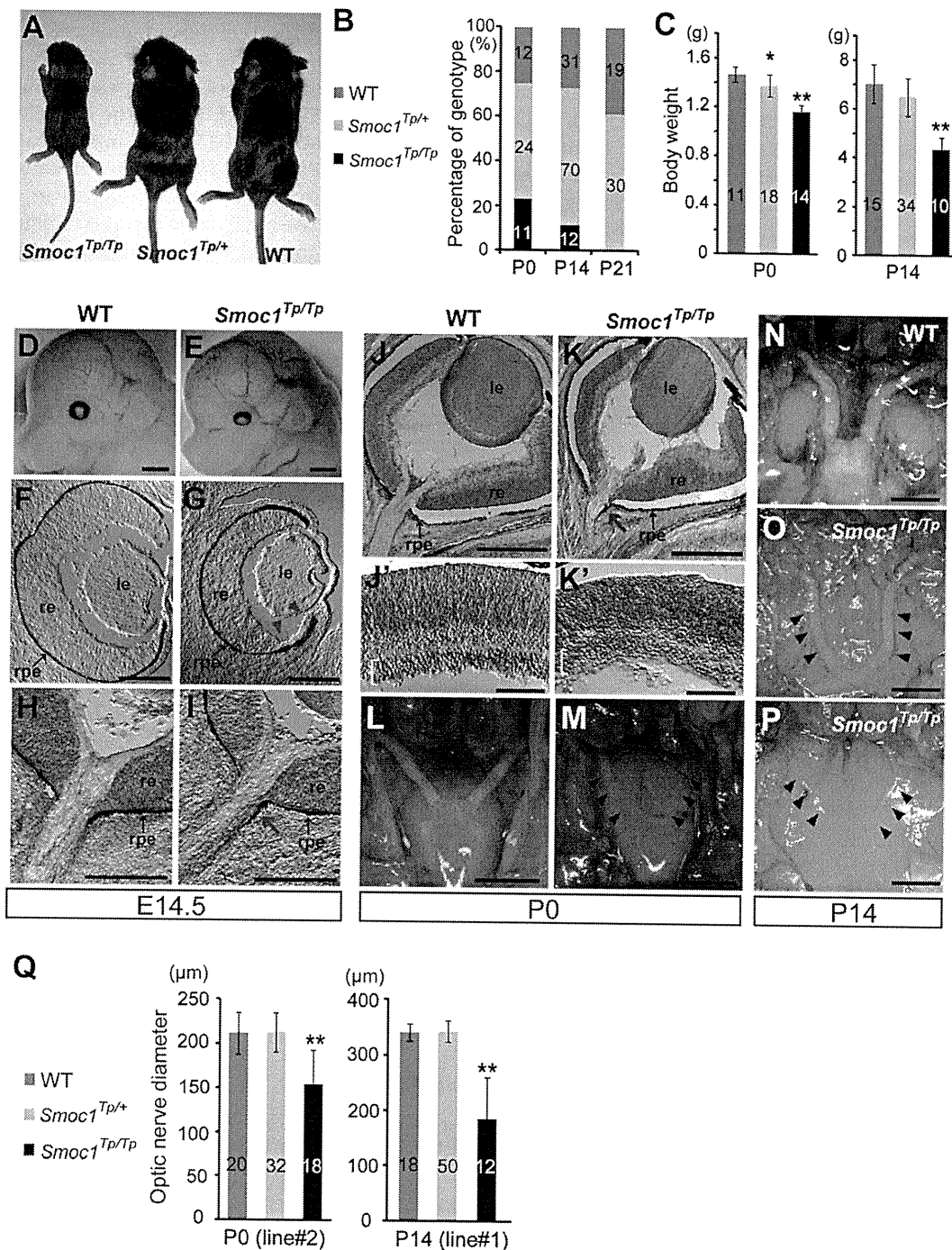
Figure 3. Growth and Ocular Phenotypes of Smoc1 Null Mice

(A) Representative Smoc1$^{Tp/Tp}$ mouse, showing a small body in comparison to Smoc1$^{Tp/+}$ and WT littermates.

(B) Genotypes of living pups during the first 3 wk of life.

(C) Body weight of pups of each genotype at P0 (left panel) and P14 (right panel).

(D and E) Relatively small eyes were evident in Smoc1$^{Tp/Tp}$ mice in comparison to WT mice.

(F–K′) Coronal sections of eyes at E14.5 (F–I) and P0 (J–K′) with TB staining (H, I, and J–K′). (F–I) Atrophy of the anteroventral part of the retina (G, magenta arrowheads, dorsal view shown at the top), hypoplastic optic nerve, and extension of the RPE to the optic nerve (I, magenta arrow) in Smoc1$^{Tp/Tp}$ mice at E14.5. (J and K) Hypoplastic optic nerve and RPE extension in Smoc1$^{Tp/Tp}$ mice at P0 (K, magenta arrow). Note that sections in which optic nerves appeared most thick are presented in (H–K). (J′–K′) In higher-magnification views of (J and K), a thinned and irregular ganglion cell layer (white brackets) was observed in Smoc1$^{Tp/Tp}$ mice. Abbreviations are as follows: le, lens; re, retina; rpe, retinal pigmented epithelium.

(L–P) Ventral views of the brain showing optic nerves at P0 (L and M) and P14 (N–P), showing various degrees of optic nerve hypoplasia.

Discussion

In a previous report, we performed parametric linkage analysis with three families (families A, B, and C) and found 16 loci showing a LOD score ($\theta = 0.000$) higher than 3.0. Additional microsatellite markers highlighted only one locus, 10p11.23.[12] However, no mutations were found in the candidate gene MPP7.[12] By recruiting a new family (family X) to this study, we successfully found homozygous mutations in SMOC1 in families A, C, and X. In family B, no SMOC1 mutations were found, indicating the genetic heterogeneity in MLA. Patients with SMOC1 mutations and Smoc1 null mice showed similar limb anomalies, such as oligodactyly, syndactyly, synostosis of 4th and 5th metacarpals, hypoplasia of fibula, and bowed tibia. Oligodactyly, syndactyly, and synostosis of 4th and 5th metacarpals are common in MLA patients.[2–4] However, hypoplastic fibula and bowed tibia are less common in patients with MLA, as four out of 34 MLA patients showed these anomalies in the previous report.[3] Although one patient with a SMOC1 mutation from family C did not show bowed tibia and hypoplastic fibula, these anomalies could be features specific to SMOC1 mutations. Further SMOC1 analysis of other MLA patients should delineate the phenotypic consequences caused by SMOC1 mutations.

Accumulating evidence suggests that BMP signaling plays crucial roles in early eye vesicle and limb patterning, skeletal formation, and apoptosis of the interdigital mesenchyme,[25–29] and mutations involving BMP signaling cause human malformations including ocular, limb, and skeletal anomalies.[7,30–33] Here, we present genetic evidence that SMOC1 is essential for ocular and limb development in humans and mice. Furthermore, Xenopus smoc can inhibit BMP signaling,[11] suggesting that SMOC1/Smoc1 can also modulate BMP signaling in humans and mice. Indeed, we observed reduced and/or disturbed expression of genes involved in BMP signaling in the interdigital mesenchyme in Smoc1 null mice, and limb and ocular abnormalities associated with loss of Smoc1 function are consistent with phenotypic consequences of disturbed BMP signaling. Conditional inactivation of Bmp2 in the limb showed 3/4 syndactyly, and a similar deficiency of both Bmp2 and Bmp7 resulted in malformed fibulae in mice.[25] Moreover, mice deficient in Fmn1, a repressor of BMP signaling, showed four digits, fused metatarsal bones, and an absence of fibulae in the hindlimbs,[34] suggesting the importance of altered BMP signaling in these features. Concerning ocular phenotypes, haploinsufficiency of mouse Bmp4 resulted in a decreased number of ganglion layer cells and absence of the optic nerve similar to Smoc1 null mice,[35] indicating that altered BMP signaling is also involved in the ocular phenotype. Interestingly, knockdown experiments of smoc by antisense morpholino in Xenopus showed absence or severe deformity of the eye and other anterior structures, which were accompanied by aberrant expression of otx2, tbx2 in the eye field.[11] Mutations of OTX2 (MIM 600037) cause micropthalmia, syndromic 5 (MCOPS5 [MIM 610125]) in humans.[36] Moreover, targeted disruption of Tbx2 resulted in a marked reduction in the size of the optic cup and a failure of optic nerve formation in mice.[37] Thus, it is possible that loss of SMOC1 function could alter the expression of OTX2 and TBX2 (MIM 600747) by disturbing BMP signaling in human developing eyes.

It is unknown how the loss of functional SMOC1, a BMP antagonist, leads to reduced expression of genes involved in BMP signaling in the interdigital mesenchyme in Smoc1 null mice. In the case of Fmn1-deficient mice, the loss of the repressor of BMP signaling resulted in downregulation of Fgf4 and Shh and in upregulation of Gremlin expression at E10.5, and absence of apoptosis of the interdigital mesenchyme between the two middle digits at E13.5.[34] Thus, there is a possibility that loss of SMOC1 could cause the imbalance among BMP, SHH, and FGF signaling, which would subsequently lead to reduced and/or disturbed expression of genes involved in BMP signaling in the interdigital mesenchyme. In fact, we observed reduced expression of Msx2 in the progressive zone of hindlimbs at E11.5 (Figure S2). Moreover, expression of Sox9, the initial cartilage condensation marker, showed abnormal limb patterning, suggesting that SMOC1 may affect BMP signaling even at early stages of limb development (Figure S3). Further examinations are required for understanding spatial and temporal actions of SMOC1/Smoc1 protein during limb development.

In conclusion, our data demonstrate that SMOC1/Smoc1 is an essential player in both ocular and limb development in humans and mice and give further support to the crucial roles of BMP signaling in these systems.

Supplemental Data

Supplemental Data include three figures and four tables and can be found with this article online at http://www.cell.com/AJHG/.

(Q) Optic nerve diameter. Optic nerves were significantly hypoplastic in $Smoc1^{Tp/Tp}$ mice in comparison to WT and $Smoc1^{Tp/+}$ littermates. The numbers of pups (B and C) or eyes (Q) corresponding to each genotype are indicated within bars. Error bars indicate standard deviation: *$p < 0.01$, compared with WT. **$p < 0.01$, compared with WT and $Smoc1^{Tp/+}$. Scale bars represent 1 mm (D, E, and L–P), 200 μm (F–I), 500 μm (J and K), and 100 μm (J' and K').
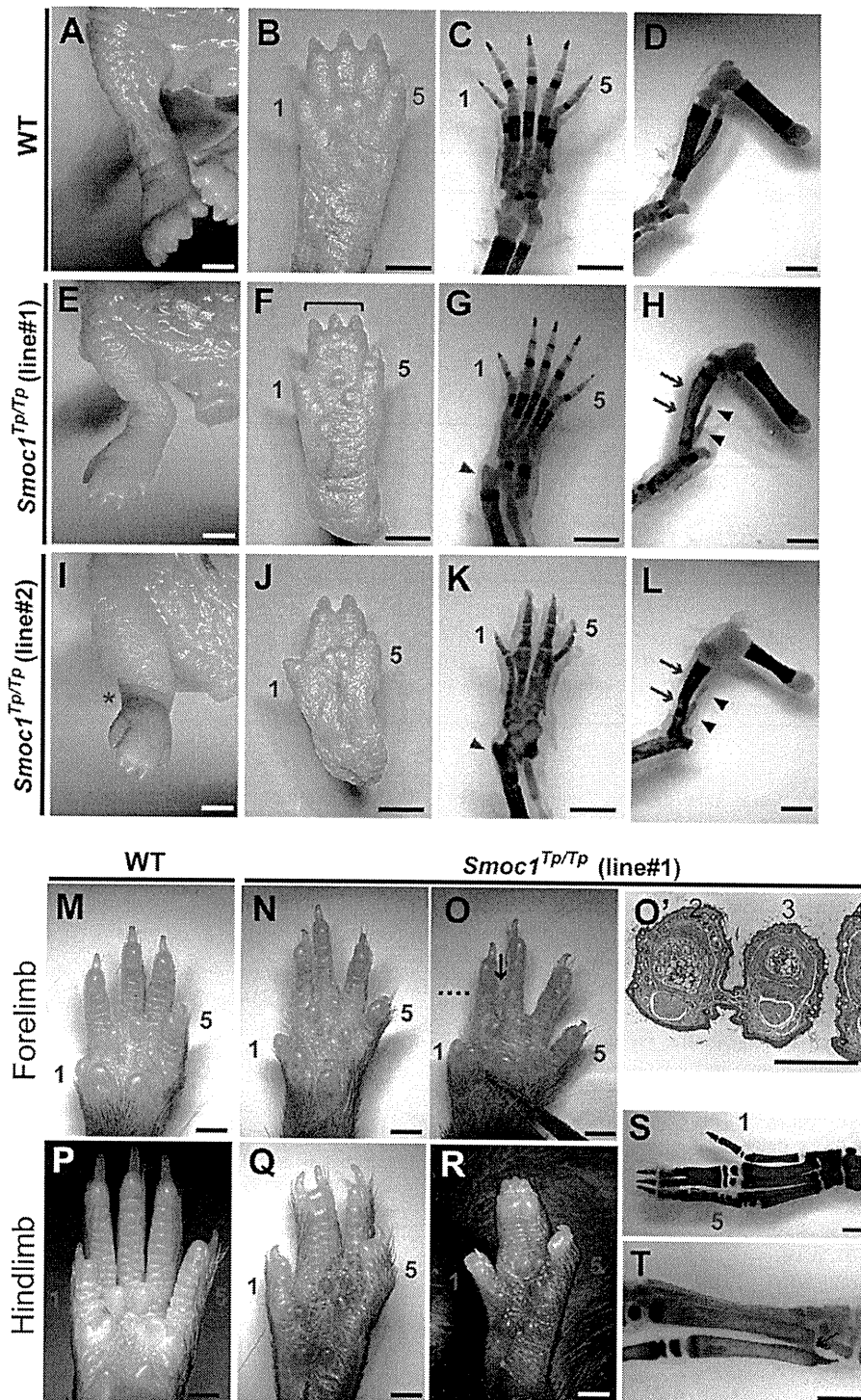
Figure 4. Limb Phenotypes of Smoc1 Null Mice

Limbs of WT (A–D, M, and P) and Smoc1[Tp/Tp] mice (E–L, N–O', and Q–T) at P0 (A–L) and P14 (M–T). Digit identities are indicated by the numbers 1 (thumb, anterior) and 5 (little finger, posterior). Skeletal staining with alcian blue and alizarin red is presented (C, D, G, H, K, L, S, and T). Smoc1[Tp/Tp] mice showed pes valgus (E and I), soft tissue syndactyly (F and G), and four digits with metatarsal fusion (J and K). Malposition of the articulation between the tibia/fibula and the calcanea (G and K, magenta arrowheads), bowed tibia (magenta arrows), and hypoplastic fibula (arrowheads) of Smoc1[Tp/Tp] mice (H and L) were observed. 2/3 soft tissue syndactyly (N) and 2/3 webbing (O) were evident in forelimbs of Smoc1[Tp/Tp] mice. (O') A transverse section taken at the level indicated by the dashed line in (O) showed 2/3 webbing. 2/3 syndactyly (Q), 2/3/4 syndactyly (R), synostosis between the 2nd and 3rd proximal phalanx and metatarsals (S), and synostosis between the 4th and 5th metatarsals (T, arrow), observed in the hindlimbs of Smoc1[Tp/Tp] mice. Scale bars represent 1 mm (A–O and P–T) or 500 μm (O').

Table 1. Limb Abnormalities in *Smoc1*$^{Tp/Tp}$ Mutants

Genotype	Talipes Valgus (No. of Affected/ Total No. of Pups)	Forelimb Abnormalities (No. of Limbs)	Hindlimb Syndactyly (No. of Limbs)					Other External Abnormalities (No. of Pups)	4th and 5th Metatarsal Fusion (No. of Affected/Total No. of Limbs)
			None	2/3[a]	3/4[b]	2/3/4[c]	4 Digits		
Postnatal Day 0									
Smoc1$^{Tp/+}$ (line 1, C57BL/6J)	0/42	0	84	0	0	0	0		
Smoc1$^{Tp/+}$ (line 2, ICR mixed)	0/38	0	76	0	0	0	0		
Smoc1$^{Tp/Tp}$ (line 1, C57BL/6J)	10/10	0	3	0	3	12	2		
Smoc1$^{Tp/Tp}$ (line 2, ICR mixed)	13/17	1[d]	1	1	9	4	19	cleft palate (3)	
Postnatal Day 14									
Smoc1$^{Tp/+}$ (line 1, C57BL/6J)	0/70	0	140	0	0	0	0		
Smoc1$^{Tp/Tp}$ (line 1, C57BL/6J)	11/11	18[e]	2	7	3	8	2	hypoplastic thumbs (5)	9/10[f]

[a] Syndactyly between the 2nd and 3rd digits.
[b] Syndactyly between the 3rd and 4th digits.
[c] Syndactyly between the 2nd, 3rd, and 4th digits.
[d] 2/3 soft tissue syndactyly.
[e] Eleven limbs showed 2/3 webbing, four limbs showed 2/3 soft tissue syndactyly, and one limb showed 3/4 syndactyly.
[f] Based on examination of skeletal preparations.

Web Resources

The URLs for data presented herein are as follows:

BDGP, http://www.fruitfly.org/
ESEfinder 3.0, http://rulai.cshl.edu/cgi-bin/tools/ESE3/esefinder. cgi?process=home
GenBank, http://www.ncbi.nlm.nih.gov/Genbank/
HSF2.4.1, http://www.umd.be/HSF/
NetGene2, http://www.cbs.dtu.dk/services/NetGene2/
Online Mendelian Inheritance in Man, http://www.ncbi.nlm.nih. gov/Omim

UCSC Genome Browser, http://genome.ucsc.edu/cgi-bin/ hgGateway
SpliceView, http://zeus2.itb.cnr.it/~webgene/wwwspliceview.html

References

1. Waardenburg, P.J. (1961). Autosomally-recessive anophthalmia with malformations of the hands and feet. In Genetics and Ophthalmology, P.J. Waardenburg, A. Franceschetti, and D. Klein, eds. (Assen, The Netherlands: Royal Van Gorcum), p. 773.

2. Teiber, M.L., Garrido, J.A., and Barreiro, C.Z. (2007). Ophthalmo-acromelic syndrome: report of a case with vertebral anomalies. Am. J. Med. Genet. A. *143A*, 2460–2462.

3. Garavelli, L., Pedori, S., Dal Zotto, R., Franchi, F., Marinelli, M., Croci, G.F., Bellato, S., Ammenti, A., Virdis, R., Banchini, G., and Superti-Furga, A. (2006). Anophthalmos with limb anomalies (Waardenburg opththalmo-acromelic syndrome): report of a new Italian case with renal anomaly and review. Genet. Couns. *17*, 449–455.

4. Tekin, M., Tutar, E., Arsan, S., Atay, G., and Bodurtha, J. (2000). Ophthalmo-acromelic syndrome: report and review. Am. J. Med. Genet. *90*, 150–154.

5. Adler, R., and Canto-Soler, M.V. (2007). Molecular mechanisms of optic vesicle development: complexities, ambiguities and controversies. Dev. Biol. *305*, 1–13.

6. Zeller, R., López-Ríos, J., and Zuniga, A. (2009). Vertebrate limb bud development: moving towards integrative analysis of organogenesis. Nat. Rev. Genet. *10*, 845–858.

7. Bakrania, P., Efthymiou, M., Klein, J.C., Salt, A., Bunyan, D.J., Wyatt, A., Ponting, C.P., Martin, A., Williams, S., Lindley, V., et al. (2008). Mutations in BMP4 cause eye, brain, and digit
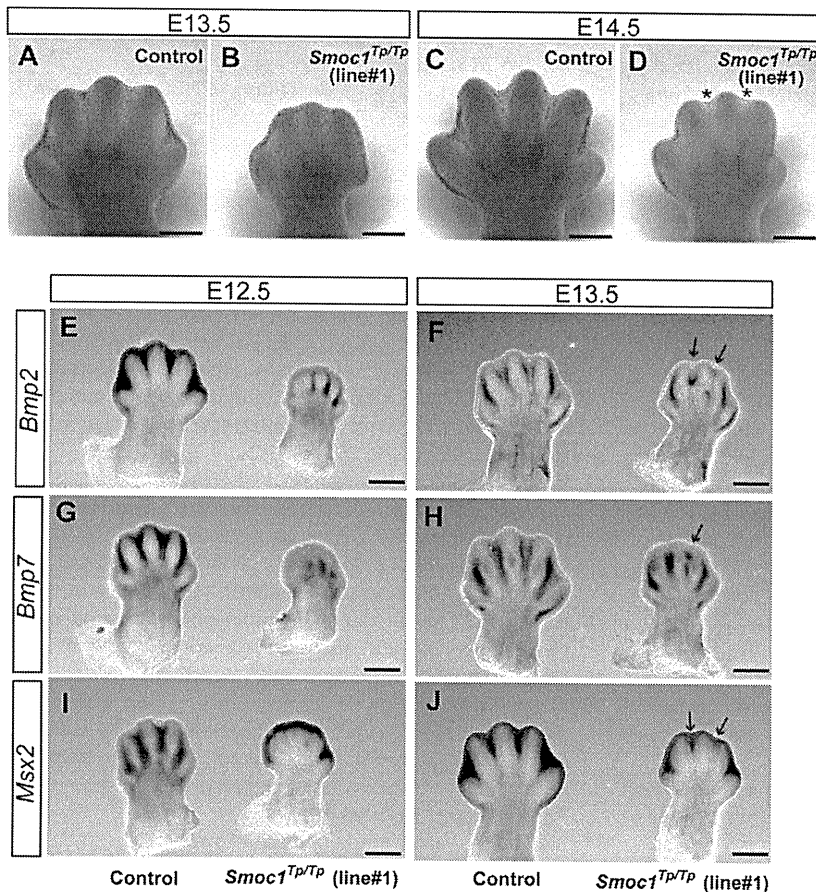
Figure 5. Reduced Apoptosis and Altered BMP Signaling in the Interdigital Mesenchyme of *Smoc1* Null Mice

(A–D) NB staining of left hindlimbs at E13.5 (A and B) and E14.5 (C and D). In comparison to control embryos (WT and *Smoc1*$^{Tp/+}$ littermates) (A and C), the number of NB-stained apoptotic cells in the interdigital mesenchyme of *Smoc1*$^{Tp/Tp}$ mice was dramatically reduced between digits 2 and 3 and digits 3 and 4 at both E13.5 and E14.5, and the webbing remained at a distal level (B and D, magenta asterisk).

(E–J) Whole-mount in situ hybridization of right hindlimbs at E12.5 (E, G, and I) and E13.5 (F, H, and J). At E12.5, interdigital expression of *Bmp2*, *Bmp7*, and *Msx2* was profoundly delayed in the hindlimbs of *Smoc1*$^{Tp/Tp}$ mice, and their expression in the interdigital mesenchyme was apparently perturbed, even at E13.5 (magenta arrows). Scale bar represents 500 μm.

developmental anomalies: overlap between the BMP4 and hedgehog signaling pathways. Am. J. Hum. Genet. *82*, 304–319.

8. Bornstein, P., and Sage, E.H. (2002). Matricellular proteins: extracellular modulators of cell function. Curr. Opin. Cell Biol. *14*, 608–616.

9. Vannahme, C., Smyth, N., Miosge, N., Gösling, S., Frie, C., Paulsson, M., Maurer, P., and Hartmann, U. (2002). Characterization of SMOC-1, a novel modular calcium-binding protein in basement membranes. J. Biol. Chem. *277*, 37977–37986.

10. Gersdorff, N., Müller, M., Schall, A., and Miosge, N. (2006). Secreted modular calcium-binding protein-1 localization during mouse embryogenesis. Histochem. Cell Biol. *126*, 705–712.

11. Thomas, J.T., Canelos, P., Luyten, F.P., and Moos, M., Jr. (2009). Xenopus SMOC-1 inhibits BMP signaling downstream of receptor binding and is essential for post-gastrulation development in Xenopus. J. Biol. Chem. *284*, 18994–19005.

12. Hamanoue, H., Megarbane, A., Tohma, T., Nishimura, A., Mizuguchi, T., Saitsu, H., Sakai, H., Miura, S., Toda, T., Miyake, N., et al. (2009). A locus for ophthalmo-acromelic syndrome mapped to 10p11.23. Am. J. Med. Genet. A. *149A*, 336–342.

13. Mégarbané, A., Souraty, N., and Tamraz, J. (1998). Ophthalmo-acromelic syndrome (Waardenburg) with split hand and polydactyly. Genet. Couns. *9*, 195–199.

14. Cogulu, O., Ozkinay, F., Gündüz, C., Sapmaz, G., and Ozkinay, C. (2000). Waardenburg anophthalmia syndrome: report and review. Am. J. Med. Genet. *90*, 173–174.

15. Miyake, N., Kosho, T., Mizumoto, S., Furuichi, T., Hatamochi, A., Nagashima, Y., Arai, E., Takahashi, K., Kawamura, R., Wakui, K., et al. (2010). Loss-of-function mutations of CHST14 in a new type of Ehlers-Danlos syndrome. Hum. Mutat. *31*, 966–974.

16. Gudbjartsson, D.F., Thorvaldsson, T., Kong, A., Gunnarsson, G., and Ingolfsdottir, A. (2005). Allegro version 2. Nat. Genet. *37*, 1015–1016.

17. Keng, V.W., Yae, K., Hayakawa, T., Mizuno, S., Uno, Y., Yusa, K., Kokubu, C., Kinoshita, T., Akagi, K., Jenkins, N.A., et al. (2005). Region-specific saturation germline mutagenesis in mice using the Sleeping Beauty transposon system. Nat. Methods *2*, 763–769.

18. Mamo, S., Gal, A.B., Bodo, S., and Dinnyes, A. (2007). Quantitative evaluation and selection of reference genes in mouse oocytes and embryos cultured in vivo and in vitro. BMC Dev. Biol. *7*, 14.

19. Parr, B.A., Shea, M.J., Vassileva, G., and McMahon, A.P. (1993). Mouse Wnt genes exhibit discrete domains of expression in the early embryonic CNS and limb buds. Development *119*, 247–261.

20. Saitsu, H., Ishibashi, M., Nakano, H., and Shiota, K. (2003). Spatial and temporal expression of folate-binding protein 1 (Fbp1) is closely associated with anterior neural tube closure in mice. Dev. Dyn. *226*, 112–117.

21. Tamplin, O.J., Kinzel, D., Cox, B.J., Bell, C.E., Rossant, J., and Lickert, H. (2008). Microarray analysis of Foxa2 mutant mouse embryos reveals novel gene expression and inductive roles

for the gastrula organizer and its derivatives. BMC Genomics *9*, 511.

22. Suzuki, D., Yamada, A., Amano, T., Yasuhara, R., Kimura, A., Sakahara, M., Tsumaki, N., Takeda, S., Tamura, M., Nakamura, M., et al. (2009). Essential mesenchymal role of small GTPase Rac1 in interdigital programmed cell death during limb development. Dev. Biol. *335*, 396–406.

23. Kimura, S., and Shiota, K. (1996). Sequential changes of programmed cell death in developing fetal mouse limbs and its possible roles in limb morphogenesis. J. Morphol. *229*, 337–346.

24. Sernagor, E., Eglen, S.J., and Wong, R.O. (2001). Development of retinal ganglion cell structure and function. Prog. Retin. Eye Res. *20*, 139–174.

25. Bandyopadhyay, A., Tsuji, K., Cox, K., Harfe, B.D., Rosen, V., and Tabin, C.J. (2006). Genetic analysis of the roles of BMP2, BMP4, and BMP7 in limb patterning and skeletogenesis. PLoS Genet. *2*, e216.

26. Robert, B. (2007). Bone morphogenetic protein signaling in limb outgrowth and patterning. Dev. Growth Differ. *49*, 455–468.

27. Dudley, A.T., Lyons, K.M., and Robertson, E.J. (1995). A requirement for bone morphogenetic protein-7 during development of the mammalian kidney and eye. Genes Dev. *9*, 2795–2807.

28. Khokha, M.K., Hsu, D., Brunet, L.J., Dionne, M.S., and Harland, R.M. (2003). Gremlin is the BMP antagonist required for maintenance of Shh and Fgf signals during limb patterning. Nat. Genet. *34*, 303–307.

29. Furuta, Y., and Hogan, B.L. (1998). BMP4 is essential for lens induction in the mouse embryo. Genes Dev. *12*, 3764–3775.

30. Asai-Coakwell, M., French, C.R., Berry, K.M., Ye, M., Koss, R., Somerville, M., Mueller, R., van Heyningen, V., Waskiewicz, A.J., and Lehmann, O.J. (2007). GDF6, a novel locus for a spectrum of ocular developmental anomalies. Am. J. Hum. Genet. *80*, 306–315.

31. Tassabehji, M., Fang, Z.M., Hilton, E.N., McGaughran, J., Zhao, Z., de Bock, C.E., Howard, E., Malass, M., Donnai, D., Diwan, A., et al. (2008). Mutations in GDF6 are associated with vertebral segmentation defects in Klippel-Feil syndrome. Hum. Mutat. *29*, 1017–1027.

32. Wyatt, A.W., Osborne, R.J., Stewart, H., and Ragge, N.K. (2010). Bone morphogenetic protein 7 (BMP7) mutations are associated with variable ocular, brain, ear, palate, and skeletal anomalies. Hum. Mutat. *31*, 781–787.

33. Ye, M., Berry-Wynne, K.M., Asai-Coakwell, M., Sundaresan, P., Footz, T., French, C.R., Abitbol, M., Fleisch, V.C., Corbett, N., Allison, W.T., et al. (2010). Mutation of the bone morphogenetic protein GDF3 causes ocular and skeletal anomalies. Hum. Mol. Genet. *19*, 287–298.

34. Zhou, F., Leder, P., Zuniga, A., and Dettenhofer, M. (2009). Formin1 disruption confers oligodactylism and alters Bmp signaling. Hum. Mol. Genet. *18*, 2472–2482.

35. Chang, B., Smith, R.S., Peters, M., Savinova, O.V., Hawes, N.L., Zabaleta, A., Nusinowitz, S., Martin, J.E., Davisson, M.L., Cepko, C.L., et al. (2001). Haploinsufficient Bmp4 ocular phenotypes include anterior segment dysgenesis with elevated intraocular pressure. BMC Genet. *2*, 18.

36. Ragge, N.K., Brown, A.G., Poloschek, C.M., Lorenz, B., Henderson, R.A., Clarke, M.P., Russell-Eggitt, I., Fielder, A., Gerrelli, D., Martinez-Barbera, J.P., et al. (2005). Heterozygous mutations of OTX2 cause severe ocular malformations. Am. J. Hum. Genet. *76*, 1008–1022.

37. Behesti, H., Papaioannou, V.E., and Sowden, J.C. (2009). Loss of Tbx2 delays optic vesicle invagination leading to small optic cups. Dev. Biol. *333*, 360–372.
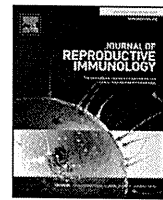
Coding region polymorphisms in the indoleamine 2,3-dioxygenase (INDO) gene and recurrent spontaneous abortion

Dawar Amani[a,*], Fatemeh Ravangard[a], Norrio Niikawa[b], Ko-ichiro Yoshiura[b], Mojtaba Karimzadeh[c], Alamtaj Samsami Dehaghani[d], Abbas Ghaderi[e,f]

[a] Department of Immunology, Medical School, Ardabil University of Medical Sciences, Ardabil, Iran
[b] Department of Human Genetics, Nagasaki University Graduate School of Biomedical Sciences, 1-12-4 Sakamoto, Nagasaki 852-8523, Japan
[c] Department of Immunology, Medical School, Uromieh University of Medical Sciences, Uromieh, Iran
[d] Department of Obstetrics and Gynecology, Medical School, Shiraz University of Medical Sciences, Shiraz, Iran
[e] Department of Immunology, Medical School, Shiraz University of Medical Sciences, P.O. Box 71345-1798, Shiraz, Iran
[f] Shiraz Institute of Cancer Research, Medical School, Shiraz University of Medical Sciences, P.O. Box 71345-1798, Shiraz, Iran

ARTICLE INFO

ABSTRACT

Indoleamine 2,3-dioxygenase (INDO) catalyzes degradation of the indole ring of indoleamines and locally depletes tryptophan. INDO expression suppresses T cell proliferation and activation. Genetic variation in the INDO gene may contribute to the variable INDO enzyme expression, activity and severity of some diseases. Recurrent spontaneous abortion (RSA) is a common pregnancy complication and the exact causes of RSA are not yet known. We performed an association study between INDO single nucleotide polymorphisms (SNPs) and RSA. To identify INDO SNPs we sequenced DNA samples for ten exons and adjacent intronic regions from 111 RSA patients. Consequently 10 SNPs were detected; four in exons (one in exon 4, two in exon 9 and one in exon 10) and six in intronic regions (one in intron 3, three in intron 6, one in intron 8 and one in intron 9). Three (IVS3+562 del C, IVS8+116 T → G and IVS9+2431 G → A) of these ten SNPs have been registered at the NCBI SNP database. Statistical analysis of allele, genotype and haplotype frequency distribution in the three most frequent SNPs (IVS3+562 del C, IVS6+61 G → A and IVS9+2431 G → A) showed no significant differences between the 111 RSA and 105 matched control women. CGA and CGG were the most frequent haplotypes in both the RSA and control groups. We conclude that there is no association between INDO polymorphisms and susceptibility of Iranian women to RSA.

© 2010 Elsevier Ireland Ltd. All rights reserved.

1. Introduction

In 1953 Medawar pointed out that survival of the allogenic mammalian conceptus contradicts the laws of tissue transplantation (Medawar, 1953). Since Medawar's publication there have been many discoveries that relate to immune regulation during pregnancy (Billington, 2003). Some of these regulatory mechanisms include: expression of non-polymorphic MHC class 1 molecules and key roles for cytokines such as IL-10 and TGFβ and Fas ligand (FasL/CD95L). All of these factors contribute to the inhibition of T cell activation at the maternal–fetal interface (Entrican, 2002).

Kamimura et al. (1991) reported a link between indoleamine 2,3-dioxygenase (INDO) expression and pregnancy success in humans. Munn et al. (1998) reported that placental expression of INDO is required to mediate tolerance by maternal CD8+ T cells specific for paternal class I

MHC. INDO is a 42 kDa cytosolic monomeric protein, which catalyzes the degradation of the indole ring of tryptophan and other indoleamines (Hayaishi, 1985). The INDO gene is located on chromosome 8 (8p12–p11) and contains 10 exons (Kadoya et al., 1992).

Although INDO was first described in 1963 and early attention focused on its role in antimicrobial resistance, the biological significance of INDO has now been examined (Taylor and Feng, 1991; Hayaishi, 1993; Mellor and Munn, 1999). The expression of INDO by dendritic cells (DCs), monocytes and macrophages results in immunomodulatory effects on T cells due to the peri-cellular degradation of the essential amino acid tryptophan (Munn et al., 1999). In a comprehensive review Grohmann et al. (2003) discussed the roles of INDO in the control of T cell activity during infection, pregnancy, autoimmunity, transplantation and neoplasia (Grohmann et al., 2003).

Recurrent spontaneous abortion (RSA) is defined as "occurrence of three or more consecutive pregnancy losses before 20 weeks of gestation, with a fetus weighing 500 g or less" (WHO Recommended Definitions, 1997; Garcia-Enguidanos et al., 2002). It is believed that approximately one in 300 women globally experiences RSA. Although various etiologic factors have been postulated, the exact underlying pathophysiologic mechanisms remain elusive in up to 40–50% of cases (Philipp et al., 2003).

In this investigation, we hypothesized that INDO gene polymorphisms and allele frequencies are different in RSA patients to normally fertile control women. To test this hypothesis, we screened INDO gene exons and adjacent intronic regions for SNPs and evaluated their frequencies in RSA patients and in matched control women.

2. Materials and methods

2.1. Subjects

The subjects consisted of 111 southern Iranian women (aged 17–38 years; mean 27.2 years) who had experienced at least three RSA (mean 3.5) and in whom anatomical, hormonal, chromosomal, infectious and autoimmune causes including anti-phospholipid syndrome, had been excluded. They all attended the Department of Obstetrics and Gynecology Clinic of Shiraz University of Medical Sciences. The control individuals consisted of 105 ethnically matched women (aged 22–50 years; mean 36.5 year) who had at least two children (mean 3.4) and no history of pregnancy

loss. The subjects and controls participated in this study after informed consent.

2.2. DNA extraction and sequencing of INDO

Venous blood was collected in EDTA-coated tubes, and DNA extracted using the salting out method (Miller et al., 1988). For detection of new single nucleotide polymorphisms (SNPs) we sequenced DNA samples from 111 RSA women for ten exons and adjacent intronic regions of the INDO gene. Forward and reverse primers specific for each exon (Nippon Gene Co. Ltd., Japan) were used in PCR in a mixture containing 25 ng DNA as template. PCR products (10 μl) were cleaned up using Exo SAP-IT enzymatic solution (Usb Corp., USA). Cleaned up PCR products were used as template in sequencing reactions. Sequencing primers (Nippon Gene Co. Ltd., Japan) and Big Dye terminator V3.1 cycle sequencing kit (PE Applied Biosystem, USA) were used in sequencing reactions according to the manufacturer's protocol. After preparation, samples were analyzed using an ABI PRISM 3100 machine. Resultant electropherograms were analyzed by DNA sequencing analysis software version 3.7 (PE Applied Biosystem). For detection of SNPs, electropherograms were aligned using of Auto-assembler version 2.1 (PE Applied Biosystem).

2.3. Statistical analysis

The frequency of each polymorphic allele was calculated by the allele counting method. Differences in the genotype and allele frequencies between patients and controls were tested by χ^2 analysis. Haplotype estimation and differences in the haplotype frequencies between RSA cases and control group were analyzed by Arlequin version 2000 software (http://anthro.unige.ch/arlequin).

3. Results

3.1. Sequencing analysis

3.1.1. SNP identification

Sequencing of ten exons and adjacent intronic regions of INDO in 111 RSA women detected 10 different base changes. These included one deletion (IVS3+562 del C) at the upstream region of exon 4, one SNP [325 G → A (Val 109 Ile)] within exon 4, three SNPs (IVS6+32 T → G, IVS6+54 T → A and IVS6+61 G → A) in intron 6, one SNP (IVS8+116

Table 1
Detected SNPs in screening of exons and adjacent intronic regions of INDO in RSA patients using automated sequencing.

| SNPs	NCBI SNP database	Position	Allele frequency (allele)
IVS3+562 del C	rs 4259403	Intron 3	0.88 (C)
325 G → A (Val 109 Ile)	a	Exon 4	0.995 (G)
IVS6+32 T → G	a	Intron 6	0.995 (T)
IVS6+54 T → A	a	Intron 6	0.99 (T)
IVS6+61 G → A	a	Intron 6	0.97 (G)
IVS8+116 T → G	rs 9298586	Intron 8	0.995 (T)
720 C → T (Asp 240 Asp)	a	Exon 9	0.995 (C)
805 G → A (Val 269 Ile)	a	Exon 9	0.995 (G)
IVS9+2431 G → A	rs 3739319	Intron 9	0.42 (G)
954 G → A (Glu 318 Glu)	a	Exon 10	0.98 (G)

a The seven novel SNPs.
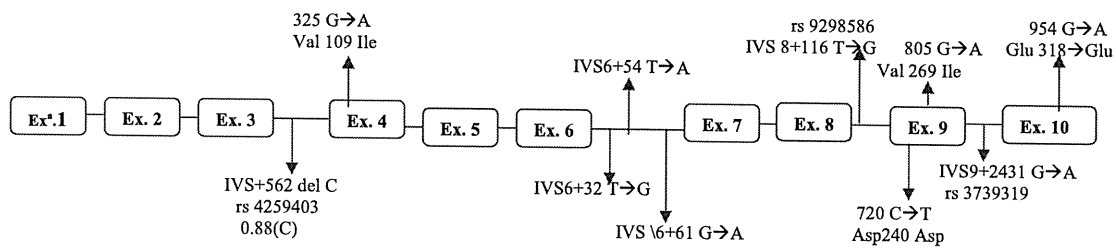
Fig. 1. Schematic illustration of the positions of detected SNPs region of *INDO* in RSA patients using automated sequencing. Ex[a]: exon.

T→ G) in intron 8, two SNPs [720 C→ T (Asp 240 Asp) and 805 G → A (Val 269 Ile)] within exon 9, one SNP (IVS9+2431 G→ A) in intron 9 and one SNP [954 G → A (Glu 318 Glu)] in exon10. Three of the detected SNPs had been registered in the Pubmed SNP database (Table 1 and Fig. 1). The one SNP at intron 6 (IVS6+32 T→ G) was only seen in the control group. Allelic frequencies of two intronic SNPs in intron 3 and 9 were 12% and 56% respectively. Also we detected two nonsynonymous SNPs in exon 4 (325 G → A Val 109 Ile) and exon 9 (805 G→ A Val 269 Ile); and two synonymous SNPs, one in exon 9 (720 C→ T Asp 240 Asp) and the other in exon 10 (954 G→ A Glu 318 Glu).

3.2. Comparison of three polymorphisms between RSA patients and control women

Three of the ten detected SNPs with high allele frequencies were chosen for a case–control association study. These SNPs were IVS3+562 del C, IVS 6+61 G→ A and IVS 9+2431 G→ A. The distribution of genotypes and allele frequencies of these three SNPs among RSA patients and the control women are summarized in Table 2. As indicated, no significant differences in genotype distributions and allele frequencies were observed between the two groups. Neither deletion-homozygosity at the IVS3+562 del C site nor AA-homozygosity at the IVS6+61 G→ A polymorphic site was found among RSA and control women.

3.3. Comparison of haplotype frequencies between RSA patients and control women

A total of 6 haplotypes were constructed at the 3 polymorphic sites among RSA and control women (Table 3). Among them, the two most frequent in both study groups were CGA and CGG. Statistical analysis showed no significant difference in their frequency distributions between

Table 2
Distribution of detected SNP genotypes and alleles in RSA patients and the control group using automated sequencing.[a]

INDO genotype and alleles	RSA patients[b] (N = 111)	Controls[b] (N = 105)	P-value
Genotype IVS3+562 del C			
CC	84 (77. 8)	86 (81)	
C*[d]	24 (22.2)	19 (19)	
**	0 (0)	0 (0)	0.32
Allele			
C	0.88	0.91	
*	0.12	0.9	0.32
Genotype IVS6+61 G→ A			
GG	97 (93.3)	95 (94)	
GA	7 (6.7)	6 (6)	
AA	0	0	0.52
Allele			
G	0.97	0.97	
A	0.03	0.03	0.66
Genotype IVS9+2431 G→ A			
GG	19 (18.6)	25 (24.27)	
GA	48 (47.1)	54 (52.42)	
AA	35 (34.3)	24 (23.3)	0.17
Allele			
G	0.42	0.51	
A	0.58	0.49	0.13

[a] Values are shown in absolute numbers (percentage).
[b] In certain SNPs the analyzed samples were less than 105 and 111 because of technical problems.
*[d]Deletion.
*Deletion of one nucleotide; **Homozygot (two nucleotide) deletion.

the two study groups (P = 0.7). None of the 2 haplotypes were associated with RSA.

4. Discussion

Indoleamine 2,3-dioxygenase (INDO) is expressed at the maternal–fetal interface and may suppress maternal

Table 3
Comparison of *INDO* haplotype frequency distributions between RSA patients and controls.

No.	IVS3+562delC	IVS6+61 G→ A	IVS9+2431 G→ A	Freq.		P-value
				RSA	Controls	
1	C	G	A	0.49	0.44	0.7
2	C	G	G	0.35	0.43	
3	*[a]	G	G	0.07	0.05	
4	*	G	A	0.05	0.05	
5	C	A	A	0.03	NS	
6	C	A	G	NS	0.03	
			Total	99	100	

NS: not seen.
*[a]: deletion.
*Nucleotide deletion.

Table 4

INDO SNP functional consequences using SNPnexsus database.

SNPname	dbSNPs	Gene	Source	Transcripts	Functional consequences (number of transcripts)	Distance to splice
IVS3+562 del C	rs 4259403	INDO	RefSeq	1	Intronic	45
			Ensembl	1	Intronic	45
			VEGA	1	Intronic	45
			UCSC	2	Intronic	45
			AceView	5	Intronic	45
		lervawbu	AceView	1	Intronic	14,749
325 G→A (Val 109 Ile)	a	INDO	RefSeq	1	Coding; NS(V 109 I)	
			Ensembl	1	Coding; NS(V 109 I)	
			VEGA	1	Coding; NS(V 109 I)	
			UCSC	2	Coding; NS(V 109 I)(l), 3UTR(1)	
			AceView	5	Coding; NS(V 109 I)(4), 5UTR(1)	
		lervawbu	AceView	1	Intronic	14,815
IVS6+32 T→G	a	INDO	RefSeq	1	Intronic	31
			Ensembl	1	Intronic	31
			VEGA	1	Intronic	31
			UCSC	2	Intronic	31
			AceView	5	Intronic(4), Coding; NS(V 190 F)(1) 31	
		lervawbu	AceView	1	Intronic	18,661
IVS6+54 T→A	a	INDO	RefSeq	1	Intronic	53
			Ensembl	1	Intronic	53
			VEGA	1	Intronic	53
			UCSC	2	Intronic	53
			AceView	5	Intronic(4), Coding; NS(N 197 I)(l) 53	
		lervawbu	AceView	1	Intronic	18,683
IVS6+61 G→A	a	INDO	RefSeq	1	Intronic	60
			Ensembl	1	Intronic	60
			VEGA	1	Intronic	60
			UCSC	2	Intronic	60
			AceView	5	Intronic(4), Coding; NS(F 197 L)(l)	60
		lervawbu	AceView	1	Intronic	18,690
IVS8+116 T→G	rs 9298586	INDO	RefSeq	1	Intronic	116
			Ensembl	1	Intronic	116
			VEGA	1	Intronic	116
			UCSC	2	Intronic	116
			AceView	5	3 downstream(3), Intronic(2)	116
		lervawbu	AceView	1	Intronic	20,867
720 C→T (Asp 240 Asp)	a	INDO	RefSeq	1	Coding; S(D240 D)	
			Ensembl	1	Coding; S(D 240 D)	
			VEGA	1	Coding; S(D240 D)	
			UCSC	2	Coding; S(D240 D)(l), 3UTR(1)	
			AceView	4	3 downstream(1), 3UTR(1), Coding; S(D240 D), S(G 93 G)(2)	
		lervawbu	AceView	1	Intronic	21,214
805 G→A(Val 269 Ile)	a	INDO	RefSeq	1	Coding; NS(V 269 1)	
			Ensembl	1	Coding; NS(V 269 1)	
			VEGA	1	Coding; NS(V 269 1)	
			UCSC	2	Coding; NS(V 269 I)(l), 3UTR(1)	
			AceView	4	3downstream(l), 3UTR, Coding(1); NS(V269I), NS(V22I)(2)	
		lervawbu	AceView	1	Intronic	21,299
IVS9+2431 G→A	rs 3739319	INDO	RefSeq	1	Intronic	28
			Ensembl	1	Intronic	28
			VEGA	1	Intronic	28
			UCSC	2	Intronic	28
			AceView	3	Intronic	28
		lervawbu	AceView	1	Intronic	23871
954 G→A(Glu 318 Glu)	a	INDO	RefSeq	1	Coding; S(E 318 E)	
			Ensembl	1	Coding; S (E 318 E)	
			VEGA	1	Coding; S(E 318 E)	
			UCSC	2	Coding; S(E 318 E)(l), 3UTR (1)	
			AceView	3	3UTR(1), Coding; S, S(E 171 E) (E318 E)(2)	
		lervawbu	AceView	1	Intronic	21,214

NS: non-synonymous; S: synonymous.

[a] Novel SNP.

immune response to the semi-allogeneic fetus (Munn et al., 1998). Recent data demonstrated that CD4+CD25+ regulatory T cells (Treg cells) and the INDO enzyme may cooperate in the induction of maternal tolerance during pregnancy (Saito et al., 2007).

Ligation of CTLA-4, which is expressed on CD4+CD25+ Treg cells, enhances INDO activity in dendritic cells (DC) and macrophages (Fallarino et al., 2003). Miwa et al. (2005) showed that INDO expression in DCs after CTLA-4 treatment is decreased in miscarriages. Therefore, CD4+CD25+ Treg cells and INDO expressing DCs are very important in the maintenance of normal pregnancy. A decreased number and reduced function of Treg cells in women with RSA has been reported (Arruvito et al., 2007). This decrease may affect INDO expression and activity and may result in immunologic pregnancy complications such as RSA. Despite these findings several investigators have reported that INDO functions as facilitator of conversion of naïve T lymphocytes into Treg cells (Fallarino et al., 2006).

In this investigation, we screened exons and exon–intron borders of the INDO gene and identified ten genetic variants in 111 southern Iranian RSA patients. In a similar study Arefayene et al. (2009) identified seventeen genetic variants of INDO in Caucasian and African–American normal subjects in USA. This group also analyzed the functional effect of different variants on INDO enzyme activity.

Three of our identified SNPs had previously been registered in the NCBI SNP database (Table 1). Two of them (rs 9298586 and rs 3739319) were also reported by the Arefayene group (Arefayene et al., 2009). In this study the allele frequency of IVS9+2431 G → A was higher than the Arefayene study (42% VS 1%) which emphasized ethnic differences. There are many other INDO SNPs in the NCBI SNP data base which were not identified in this investigation, because they probably exist in certain regions of the gene that were not sequenced, or alternatively they are lacking in Iranian women. Additional studies are needed to clarify the presence of INDO gene variants in other populations.

For functional annotation of both new and known identified INDO gene SNPs in this study, we used the SNPnexus database. This database is the only tool that provides a comprehensive overview of functional consequences of SNPs on alternatively spliced genes by exploring five different transcriptome and proteome models (Chelala et al., 2008). The results of analysis of the 10 identified SNPs of INDO using the SNPnexus database are summarized in Table 4. Two of five models (UCSC and AceView) utilized by SNPnexus database showed more than one functional consequence, e.g. 3UTR, 5UTR and 3downstream. According to the AceView models INDO variants overlap with isoforms of the lervawbu gene. The distance from splicing sites of intronic SNPs are detailed in Table 4.

To the best of our knowledge and as confirmed by the SNPsnexus database analysis, there is no report in the literature concerning an association between INDO polymorphisms, haplotypes and RSA, therefore we were not able to make a comparative analysis.

In conclusion, according to this study INDO exhibits different genetic variants in different populations and there is no association between INDO polymorphisms and RSA.

Other investigations are needed to clarify the genetic variants of INDO in different ethnic groups and the association of its polymorphism with RSA.

References

Arefayene, M., Philips, S., Cao, D., Mamidipalli, S., Desta, Z., Flockhart, D.A., et al., 2009. Identification of genetic variants in the human indoleamine 2,3-dioxygenase (INDO1) gene, which have altered enzyme activity. Pharmacogenet. Genomics 19 (6), 464–476.

Arruvito, L., Sanz, M., Banham, A.H., Fainboim, L., 2007. Expansion of CD4+ CD25+ and FOXP3+ regulatory T cells during the follicular phase of the menstrual cycle: implications for human reproduction. J. Immunol. 178 (4), 2572–2578.

Billington, W.D., 2003. The immunological problem of pregnancy: 50 years with the hope of progress. A tribute to Peter Medawar. J. Reprod. Immunol. 60, 1–11.

Chelala, C., Khan, A., Lemoine, N.R., 2008. SNPnexus: a web database for functional annotation of newly discovered and public domain Single Nucleotide Polymorphisms. Bioinformatics 25 (5), 655–661.

Entrican, G., 2002. Immune regulation during pregnancy and host–pathogen interactions in infectious abortion. J. Comp. Pathol. 126, 79–94.

Fallarino, F., Grohmann, U., Hwang, K.W., Orabona, C., Vacca, C., Bianchi, R., et al., 2003. Modulation of tryptophan catabolism by regulatory T cells. Nat. Immunol. 4, 1206–1212.

Fallarino, F., Grohmann, U., You, S., McGrath, B.C., Cavener, D.R., Vacca, C., et al., 2006. The combined effects of tryptophan starvation and tryptophan catabolites down-regulate T cell receptor zeta-chain and induce a regulatory phenotype in naive T cells. J. Immunol. 176 (11), 6752–6761.

Garcia-Enguidanos, A., Calle, M.E., Valero, J.A., Luna, S., Domínguez-Rojas, V., 2002. Risk factors in miscarriage: a review. Eur. J. Obstet. Gynecol. Reprod. Biol. 102 (2), 111–119.

Grohmann, U., Fallarino, F., Puccetti, P., 2003. Tolerance, DCs and tryptophan: much ado about INDO. Trends Immunol. 24 (5), 242– 248.

Hayaishi, O., 1985. Indoleamine 2, 3-dioxygenase—with special reference to the mechanism of interferon action. Biken J. 28 (1–2), 39–49.

Hayaishi, O., 1993. My life with tryptophan—never a dull moment. Protein Sci. 2, 472–475.

Kadoya, A., Tone, S., Maeda, H., Minatogawa, Y., Kido, R., 1992. Gene structure of human indoleamine 2,3-dioxygenase. Biochem. Biophys. Res. Commun. 189 (1), 530–536.

Kamimura, S., Eguchi, K., Yonezawa, M., Sekiba, K., 1991. Localization and developmental change of indoleamine 2,3-dioxygenase activity in the human placenta. Acta Med. Okayama 45, 135–139.

Medawar, P.B., 1953. Some immunological and endocrinological problems raised by the evolution of viviparity in vertebrates. Symp. Soc. Exp. Biol. Med. 7, 320–338.

Mellor, A.L., Munn, D.H., 1999. Tryptophan catabolism and T-cell tolerance: immunosuppression by starvation? Immunol. Today 20, 469–473.

Miller, S.A., Dykes, D.D., Polesky, H.F., 1988. A simple salting out procedure for extracting DNA from human nucleated cells. Nucleic Acids Res. 16, 1215.

Miwa, N., Hayakawa, S., Miyazaki, S., Myojo, S., Sasaki, Y., Sakai, M., et al., 2005. INDO expression on decidual and peripheral blood dendritic cells and monocytes/macrophages after treatment with CTLA-4 or interferon-gamma increase in normal pregnancy but decrease in spontaneous abortion. Mol. Hum. Reprod. 11, 865–870.

Munn, D.H., Zhou, M., Attwood, J.T., Bondarev, I., Conway, S.J., Marshall, B., Brown, C., Mellor, A.L., 1998. Prevention of allogeneic fetal rejection by tryptophan catabolism. Science 281, 1191–1193.

Munn, D.H., Shafizadeh, E., Attwood, J.T., Bondarev, I., Pashine, A., Mellor, A.L., 1999. Inhibition of T cell proliferation by macrophage tryptophan catabolism. J. Exp. Med. 189, 1363–1372.

Philipp, T., Philipp, K., Reiner, A., Beer, F., Kalousek, D.K., 2003. Embryoscopic and cytogenetics analysis of 233 missed abortions: factors involved in the pathogenesis of developmental defects of early failed pregnancies. Hum. Reprod. 18, 1724–1732.

Saito, S., Shima, T., Nakashima, A., Shiozaki, A., Ito, M., Sasaki, Y., 2007. What is the role of regulatory T cells in the success of implantation and early pregnancy? J. Assist. Reprod. Genet. 24 (9), 379– 386.

Taylor, M.W., Feng, G.S., 1991. Relationship between interferon-γ, indoleamine 2,3-dioxygenase, and tryptophan catabolism. FASEB J. 5, 2516–2522.

WHO Recommended Definitions, 1997. Terminology and format for statistical tables related to the prenatal period. Acta Obstet. Gynecol. Scand. 56, 247–253.

N. Ahmad Aziz, PhD,[1] Hanno Pijl, MD, PhD,[2]
Marijke Frölich, PhD,[3] Ferdinand Roelfsema, MD, PhD,[2]
Raymund A.C. Roos, MD, PhD[1]

[1]Department of Neurology,
[2]Department of Endocrinology and
Metabolic Diseases,
[3]Department of Clinical Chemistry,
Leiden University Medical Center,
Leiden, The Netherlands

References

1. Aziz NA, van der Marck MA, Pijl H, Olde Rikkert MG, Bloem BR, Roos RA. Weight loss in neurodegenerative disorders. J Neurol 2008;255:1872–1880.

2. Trujillo ME, Scherer PE. Adipose tissue-derived factors: impact on health and disease. Endocr Rev 2006;27:762–778.

3. Evidente VG, Caviness JN, Adler CH, Gwinn-Hardy KA, Pratley RE. Serum leptin concentrations and satiety in Parkinson's disease patients with and without weight loss. Mov Disord 2001;16:924–927.

4. Fiszer U, Michalowska M, Baranowska B, et al. Leptin and ghrelin concentrations and weight loss in Parkinson's disease. Acta Neurol Scand 2010;121:230–236.

5. Lorefalt B, Toss G, Granerus AK. Weight loss, body fat mass, and leptin in Parkinson's disease. Mov Disord 2009;24:885–890.

6. Signore AP, Zhang F, Weng Z, Gao Y, Chen J. Leptin neuroprotection in the CNS: mechanisms and therapeutic potentials. J Neurochem 2008;106:1977–1990.

7. Aziz NA, Pijl H, Frolich M, van der Graaf AW, Roelfsema F, Roos RA. Leptin secretion rate increases with higher CAG repeat number in Huntington's disease patients. Clin Endocrinol (Oxf) 2010;73:206–211.

Mutation and Copy Number Analysis in Paroxysmal Kinesigenic Dyskinesia Families

Paroxysmal kinesigenic dyskinesia (PKD [MIM128200]) is a heritable paroxysmal movement disorder characterized by recurrent and brief attacks of involuntary movements.[1,2] Its family histories show an autosomal dominant inheritance

*Correspondence to: Akira Kinoshita, Department of Human Genetics, Nagasaki University Graduate School of Biomedical Sciences, Nagasaki, Japan; akino@nagasaki-u.ac.jp

pattern. Our previous linkage and haplotype analyses defined the disease locus on 16p11.2-q12.1,[2] Similarly, other linkage studies of PKD assigned the locus to an overlapping region encompassing the centromere of chromosome 16.[3–5] In our previous study, we performed mutation analysis in seven families on 157 genes between D16S3131 and D16S416 (all the genes within this region); however, we failed to identify the causative gene.[1] Based on many linkage studies, we decided to extend the candidate region until more telomeric locus to D16S503 containing 72 RefSeq genes. Because genomic rearrangement could also result in PKD, we also performed copy number analysis for the entire candidate PKD locus.

Here, we describe the results of mutation analysis in 14 PKD families for the 72 genes between D16S416 and D16S503, and the results of copy number analysis in eight PKD families and two sporadic cases.

We collected 14 Japanese families, PKD-1–PKD-14, each of which includes multiple individuals affected by PKD, and two sporadic cases, PKD-S1 and PKD-S2. Among all these families, 64 patients were diagnosed with PKD. Our previous study showed that all affected members in each family have a disease related haplotype on chromosome 16[1,2] except for PKD-1 and PKD-2, which were not analyzed for haplotype because the family members is small.

Direct sequencing of the 72 genes in the segment between D16S416 and D16S503 revealed two substitutions which were not observed among 288 normal controls and not deposited in dbSNP (http://www.ncbi.nlm.nih.gov/SNP/) (Table 1). A substitution, g.25190C>T (p.R282C) in *GPR114* found in the family PKD-12, was considered as rare variant because it was not co-segregated with PKD. The remaining one was g.35905C>T in exon 4 of *NLRC5* (NM_032206) resulting in p.T153T, segregated with PKD in family PKD-3. Even though this mutation in *NLRC5* is "silent," it might be a pathogenic because of splicing disturbance.[6] However, a nucleotide g.35905C in *NLRC5* is not so highly conserved in other species, and g.35905C>T would not affect splicing by prediction of NNSPLICE (http://www.fruitfly.org/seq_tools/splice.html) and GENSCAN (http://genes.mit.edu/GENSCAN.html; data not shown).

Copy number analysis using HumanExon510S-Duo BeadChip (Illumina, San Diego, CA) showed a deletion in 16p11.2 (Fig. 1A), but this has already been reported in the Database of Genomic Variants (DGV) (http://projects.tcag.ca/variation/). In our previous study, two nonsynonymous substitutions, p.P242T in *SCNN1G* and p.K1063R in *ITGAL*, which were segregated with PKD in one family, were still possible pathogenic mutation for PKD.[1] Structural variants including microdeletions/microduplications within three genes, *ITGAL*, *SCNN1G*, and *NLRC5*, were scanned using array comparative genomic hybridization (aCGH: Agilent Technologies, Santa Clara, CA). Two small deletions not registered in DGV were found within *ITGAL* among several patients (Fig. 1B). However, real-time quantitative PCR revealed genomic alterations in only one PKD patient in the ITGAL region1 and region2 (Fig. 1C). No alteration was found in *SCNN1G* and *NLRC5*. Results of copy number analyses showed no causative copy number changes.

Together with our previous study,[1] we have now analyzed almost all the exons and exon-intron boundaries between